Melting of large Pt@MgO(100) icosahedra

K.Rossi[1], T.Ellaby[1], L.O. Paz-Borbón [1,2], I. Atanasov[3], L. Pavan[1], and F. Baletto[1]

E-mail: francesca.baletto@kcl.ac.uk

Abstract. We present a new parametrisation of the Vervisch-Mottet-Goniakoski (VMG) potential [Vervisch et al. Phys. Rev B24, 245411 (2002)], based on *ab-initio* density functional theory simulations for modelling oxide - metal interaction in supported nanoparticles. We apply this model to study the melting behaviour of large platinum icosahedral architectures deposited on the pristine MgO(100). Before melting, the nanoparticle undergoes two solid-solid transitions: the "squarisation" of the interface layer, followed by the full reshaping towards a truncated octahedral morphology. In between, a quite long-lived intermediate state with a (100) interface but with an icosahedral cap is observed. Our approach is shown to reproduce experimental observations, including wetting behaviour and the lack of surface diffusion.

*Keywords*Pt clusters, MgO, melting

1. Introduction

Free, supported and encapsulated metallic nanoparticles (mNPs) receive a remarkable amount of interest because of their applications in various fields, ranging from nanocatalysis to biomedicine. At the nanoscale, significant surface and interface energetic contributions, together with the lack of translation symmetry in the systems, give raise to a multi-funnel energy landscape where a variety of morphology is accessible. Hence, there is opportunity for tuning mNPs' chemophysical properties by controlling their architecture. This possibility has stimulated a threefold research line: elucidating the correlation between shape and specific properties; [1, 2, 3, 4, 5] sampling the potential energy surface of a variety of systems to identify different motifs and equilibrium structures;[6, 7, 8] addressing the coexistence of different morphology by understanding shape fluctuations and elucidating the morphological rearrangement mechanisms, of kinetically and entropically trapped metastable motifs.[9, 10, 11, 6, 12] Yet, the formation/nucleation of geometrical monodisperse samples and control over their shape has not been reached. On this regards, computational tools can provide a profound understanding of the kinetic, energetic and thermodynamics of metallic nanoparticles thus providing an aid in designing performant and stable mNPs, more readily than what could be done in laboratory experiments, and in the development of a method of production.

Previous experiments indicated that epitaxial effects dictate a shift in physical quantities, such as the melting transition, and/or the stabilisation of a phase towards another one: the thermodynamics of the nano-object can be strongly affected by the nature of its surface, e.g. exposed facets, presence of surfactants, strong interaction with the substrate. [13, 14] The melting of supported mNPs is characterised by peculiar properties such as a negative thermal expansion (e.g. a contraction of the first peak in the pair distribution function) as observed for small Pt clusters on alumina at high temperatures, [15, 16] and the detection of superheated states for both free and supported clusters. [16, 17] The effects of cluster-substrate interactions on the melting of metallic NPs is often studied on the case of bulk-like (FCC) shapes . [18, 19, 20] A single study discussed decahedral Pd on graphite, highlighting the possibility of a double melting transition with a metastable Dh cluster first melting and then recrystallising into a bulk-like (FCC) structure. [21] Up to our knowledge, no investigations relative to the thermodynamical stability icosahedral motifs has been reported notwithstanding this structure being often entropically and energetically favourable, especially below

† † Electronic Supplementary Information (ESI) available: [details of any supplementary information available should be included here]. See DOI: 10.1039/b000000x/

† [1] *School of Natural and Mathematical Sciences, Physics Department, King's College London, Strand Campus, London, WC2R 2LS, United Kingdom*

† [2] *Instituto de Fsica, Universidad Nacional Autnoma de Mxico, Apdo. Postal 20-364, 01000 Mxico, D.F. Mxico*

† [3] *Institute of Electronics, Bulgarian Academy of Sciences, 72 Tzarigradsko Chaussee Blvd, 1784 Sofia, Bulgaria*

4 nm, in the gas phase for a variety of noble and quasi-noble metal systems.

In the last couple of years, many studies focused on solid-solid structural transitions in the gas phase. [22, 23, 12]. They proved that the transition to/from the icosahedral (Ih), decahedral (Dh) and cubooctahedral (Co) basins can take place throughout a diamond-square mechanism, without the formation of any amorphous states. This concerted and cooperative process can take place only at small sizes, before atomic surface diffusion mechanisms prevail. [24, 22] On the other hand, only a few theoretical studies addressed how the geometrical distortion induced by the support epitaxy could affect the kinetic, energetic and thermodynamics of metallic nanoparticles. [18, 25, 26] Size and substrate interaction strength dependent structural transitions have been observed, while rearrangement towards equilibrium structures as predicted by Wullf-Kaishew method have been reported only in small systems and not in larger ones. [27, 13]

In this work, we propose an extension of the Vervisch-Mottet-Goniakoski (VMG) potential to allow the study of the melting of large platinum icosahedra soft-landed on the pristine MgO(100). Classical molecular dynamics (cMD) is capable of dealing with large systems (several nm in diameter), as well as finite temperatures, but requires very careful choice of the interparticle potentials and/or force fields applied. On the other hand, density functional theory (DFT) has proven successful at predicting chemophysical properties of nanoclusters, though it is very limited in terms of the size of the systems it can consider. Yet DFT data can be used to fit a still accurate and transferable empirical potential to be exploited in a cMD framework. To that end, producing a reliable description of the behaviour of supported nanoclusters of sizes upwards of 3 nm in diameter would greatly aid the *in-silico* screening and design of next generation nanodevices. Here, we focus on the case of platinum clusters, strongly interacting with a metal oxide substrate (MgO). [28, 29, 30, 31] The proposed extension consists in the introduction of a smoothing function for counting the metallic coordination so to allow a dynamical description. We show that the melting of an Ih architecture is characterized by two negative specific heat peaks. The first corresponds to the formation of a partial Ih with a (100) interface, in agreement with basin hopping calculations, [32] which survives up to 900-950 K when it transforms into an FCC-like architecture. The melting transition happens well above 1500 K, which is considerably higher than in the gas phase (1300-1350 K). The structural transitions before the melting could be described as a change of the cluster surface from a spherical "balloon" shape into a "haystack". The manuscript is organised as follows: after the description of the extension of the VMG potential, we outline our DFT simulations and the fitting procedure in the Methodology section; then we analyse and discuss the melting behaviour of large icosahedral clusters onto MgO(100) in the Results section.

2. Methodology

To model the melting behaviour of Pt nanoparticles large as 2-3 nm and deposited on an oxide surface, we propose a modification of the Vervisch-Mottet-Goniakoski

(VMG) potential [33]. It is a simple and elegant energetic model firstly developed for elucidating the microscopic origin of the cohesion on Pd-oxide interface. It introduces a Morse-like function to describe the interaction of metal nanoparticles upon MgO(100) [34, 32, 35, 36]. This approach was successfully used for identifying the lowest energy configurations for mono and bimetallic nanoparticles supported on MgO [37, 38, 39] as well as for their solidification process [27].

In the VMG force files, a periodic cosine function reproduces the MgO-checkboard on the x, y directions while the z-dependence follows a Morse-like function. In its original formulation, the energy of each metallic atom i with coordinates (x_i, y_i, z_i) and its metallic coordination CN_i is given by:

$$E^i_{M@MgO}(x_i, y_i, z_i, CN_i) = a_{i,1}\{e^{-2a_{i,2}(z_i - a_{i,3})} + 2e^{a_{i,2}(z_i - a_{i,3})}\} \quad , \tag{1}$$
$$a_{i,\alpha} = a_\alpha(x_i, y_i, CN_i) \quad \text{, with } \alpha = 1,2,3 \text{ and } i \in 1,...,\text{N}$$

where CN_i is a discrete number corresponding to the number of metallic nearest neighbours within the cluster, usually taken less than 12. Eq. 1 is a relatively simple formula to describe the influence of the substrate in the direction z perpendicular to the support. A dimensional analysis of the set of $a_{i,\alpha}$ coefficients suggests that $a_{i,1}$ tunes the strength of the interaction (in eV); $a_{i,3}$ adjusts the length along z of the interaction (in Å); while $a_{i,2}$ is the reciprocal of a length (1/Å). Those coefficients encode both the information on the metallic coordination CN_i and on the substrate geometry with respect to the atomic coordinates (x_i, y_i):

$$a_{i,\alpha}(x_i, y_i, CN_i) = b_{i,\alpha,1} + b_{i,\alpha,2}e^{-CN_i/b_{i,\alpha,3}} \quad . \tag{2}$$

The x_i and y_i coordinates of each metallic atom i lie along axes parallel to the (100) substrate. The parameters $b_{i,\alpha,\beta} = b_{\alpha,\beta}(x_i, y_i)$ describe the geometry of the substrate, and the periodicity of the checkerboard MgO(100) surface is given by a combination of sine/cosine in terms of the MgO lattice parameter $a = a_{MgO}\sqrt{2}$,

$$b_{\alpha,\beta}(x_i, y_i) = c_{\alpha,\beta,1} + c_{\alpha,\beta,2}\left[cos\left(\frac{2\pi}{a}x_i\right) + cos\left(\frac{2\pi}{a}y_i\right)\right] \tag{3}$$
$$+c_{\alpha,\beta,3}\left[cos\left(\frac{2\pi}{a}(x_i + y_i)\right) + cos\left(\frac{2\pi}{a}(x_i - y_i)\right)\right] \quad .$$

The modelling via a VMG potential leads to the fitting of the 27 parameters labelled as $c_{\alpha,\beta,\gamma}$. One should note that $c_{\alpha,3,\gamma}$ are dimensionless and they tune the screening due to the metallic coordination. On the other hand, $c_{1,1,\gamma}$ and $c_{1,2,\gamma}$ are supposed to change the strength of the interaction; $c_{3,1,\gamma}$, $c_{3,2,\gamma}$ are in Å and they control the height from the support the cluster felts it. $c_{2,1,\gamma}$ and $c_{2,2,\gamma}$, in 1/Å , tune the screening of the support interaction. Coefficients with $\gamma = 2, 3$ tailor the lateral contributions from the substrate.

The proposed extension of the VMG force field is intended to the study of dynamical properties of supported platinum clusters, including their melting behaviour. For avoiding any discontinuity of the VMG potential, instead of using a sharp cutoff distance, r_c, to define the number of nearest neighbour CN_i, a continuous and smooth function

has been introduced to calculate the metallic coordination CN_i. Following the recipe suggested in Ref. [40], it is implemented by means of a Fermi distribution function:

$$CN_i = \sum_{j \neq i} \frac{1}{1 + e^{m(\frac{r_{ij}}{r_c} - 1)}} \quad . \tag{4}$$

The sum is over all nearest neighbours j of atom i with a pair distance r_{ij}. The cutoff radius, r_c, and exponent m -which controls the smoothness of the curve- are the two parameters of the metallic coordination function, and they are fitted together with the $c_{\alpha,\beta,\gamma}$ coefficients in Eq. 3.

The fitting of these coefficient follows accurate density functional calculations, as described in the next section, and it is meant to reproduce the adhesion properties of a rich variety of configurations, represented by the selection of structures depicted in Fig. 1. In the limit of large m, the original VMG is recovered. The adhesion energy per interface atom, E_{adh}, is calculated as total energy differences between the interacting ($E_{M@MgO}$) and both the relaxed gas-phase metal cluster (E_M), and MgO(100) surface

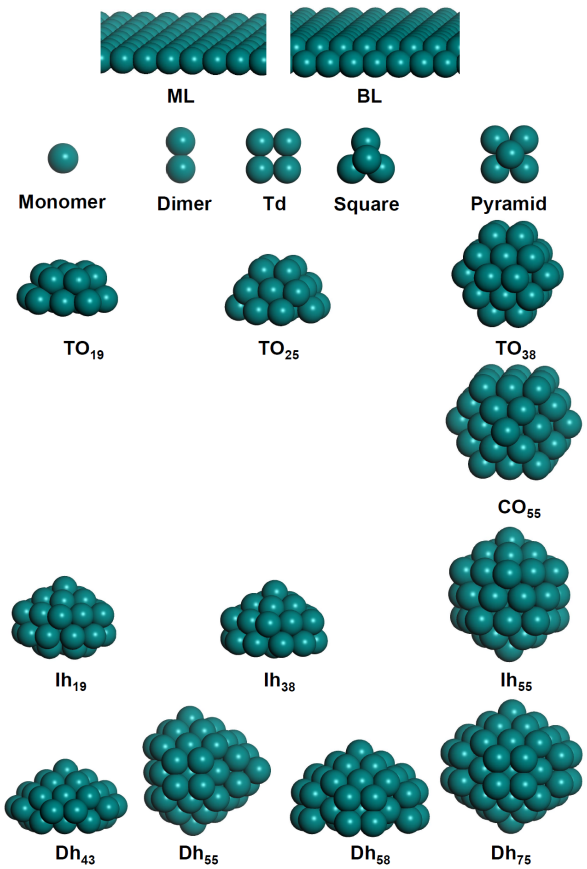

Figure 1. DFT relaxed configurations for supported Pt clusters which have been deposited on the pristine MgO(100). Size range displayed is from monomer to 75 atoms and the mono- and bi-layer in the top row. For the sake of clarity the MgO substrate is not shown.

(E_{MgO}) configurations:

$$E_{adh} = \frac{E_{M@MgO} - (E_{Metal} + E_{MgO})}{N_{interface}} \quad , \tag{5}$$

where negative E_{adh} values indicate favourable (exothermic) adsorption and $N_{interface}$ is the number of metallic atomic at the oxide interface.

The eighteen considered configurations range from the adatom, monolayer (ML), bilayer (BL) up to clusters with 75 atoms, as depicted in Fig. 2. They include subsets and complete shells of: (i) fcc-type truncated octahedral (TO) at sizes 19, 25 and 38 and cuboctahedral (CO), at size 55; (ii) non-crystallographic arrangements such as icosahedral (Ih) at sizes 33, 38 and 55; (iii) decahedral (Dh) at sizes 43, 55, 58 and 75. Data for each of the systems at O, Mg and hollow sites, have been included in the fitting set, following the original VMG methodology and Ref. [40]. Explicitly considering nanoparticles landed exposing both a (100) or a (111) facet at the oxide surface. Thus having (111)-type or other type of non-commensurate interfacial geometries, enables to account for several epitaxial geometries and makes the overall parametrisation more reliable in describing structural rearrangements taking place at the oxide surface.

2.1. Density functional simulations

We characterise various supported Pt systems on MgO(100) (Fig. 1) via extensive density functional theory (DFT) simulations, within the Quantum Espresso code [41]. The Perdew−Burke−Ernzerhof (PBE) approximation is used for the exchange and correlation functional term.[42] Rappe-Rabe-Kaxiras-Joannopoulos and Vanderbilt ultrasoft pseudo-potentials are used for describing Pt, Mg and O. The number of electrons treated variationally are: Pt($5d^9$ $6s^1$), Mg($2p^6$ $3s^1$ $3p^{0.75}$) and O($2s^2$ $2p^4$), respectively. Non-linear core corrections are included. A plane-wave energy and charge density cut-off of 45 Ry and 360 Ry are used. To improve convergence, a Marzari-Vanderbilt smearing parameter of 0.002 Ry is used. Structural relaxations are converged when forces are smaller than 0.001 $\AA/eV$, with electronic total energy differences of 10^{-5} eV. The pristine surface of MgO(100) is modelled by a 6x6 supercell in a slab configuration using three atomic layers, with a lattice constant of 4.238 Å. This is marginally larger than the experimental value of 4.21 Å, though in close agreement with previous PBE calculations (4.26 Å and 4.30 Å) and hybrid PBE0 functionals (4.21 Å).[34] The size of the unit cell provides a minimum distance between lateral images of 6.5 Å, even for the largest cluster size here considered (Pt_{75}). A vacuum of 25 Å assures that distances between images on the z-axis are located at no less than 14 Å. This provides a sufficient distance to avoid any spurious interactions between periodic images. Due to the magnetic nature of the chemical species considered, all calculations have been performed spin polarised, evaluated at the Γ-point only. After a relaxation in the gas-phase, the selected clusters have been deposited on the pristine MgO(100) surface at ∼2 Å from the substrate, maximising the number of metal-oxygen bonds at

Table 1. Structural characterisation of Pt_N clusters supported on the pristine MgO(100) surface. Normalized adhesion energy, E_{ads} (in eV), roughness of the first layer in contact with the oxide, contact angles of the different facets, average bond of the inter-metallic distances and the interface are reported. All quantities are calculated according to the definition in the text and refer to DFT-PBE relaxed configurations.

Pt_N /Shape	Interface	Roughness (std. dev.)	$N_{interface}$ Interfacial atoms	Contact angle ($\angle_{min}/\angle_{max}$)	Interfacial ave. bond (Å)	E_{ads} (PBE) (eV)
19 TO	100	0.212	9	87°/131°	2.716	-0.67
25 TO	100	0.079	12	99°/128°	2.688	-0.66
33 Ih	111	0.284	14	90°/122°	2.720	-0.51
38 Ih	111	0.241	7	89°/109°	2.647	-0.54
38 TO	100	0.011	4	51°/53°	2.854	-0.92
38 TO	111	0.226	6	49°/92°	2.785	-0.67
43 Dh	111	0.179	10	33°/108°	2.757	-0.52
55 CO	100	0.087	9	68°/96°	2.778	-0.71
55 CO	111	0.048	6	52°/82°	2.801	-0.72
55 Ih	111	0.120	7	35°/104°	2.859	-0.84
55 Dh	100	0.067	8	60°/90°	2.809	-0.84
58 Dh	111	0.219	14	102°/117°	2.766	-0.53
75 Dh	111	0.139	8	37°/78°	2.812	-0.50

the interface prior full DFT relaxation of the combined system. The 2 Å reference is based on the calculated DFT heights of a Pt atom at the O-site, which is 1.985 Å .

Values of the DFT results are summarised in Table 1. Geometrical quantities, such as the number of atoms at the interface, roughness of the interfacial layer, defined as the mean deviation from the Pt/Mg-site optimal height set at 2.688 Å , and Contact angles ($\angle$), defined as the angle formed between the substrate and the nanoparticle facets in contact with the MgO, are also reported. Single-point calculations are then performed on the relaxed configurations to account for dispersion effects using the semi-empirical approach proposed by Grimme [43]. We observe an overall increase in the adhesion energy values, from 0.34 to 0.67 eV for the ultra-nano Pt clusters (dimer to pentamer), and from 0.71 to 1.28 eV for sizes above 19 atoms. An influence of dispersion effects on adhesion energies has been recently reported for supported Pt clusters over graphene. [44] However, the general trends of the adhesion energy is maintained and most importantly the relaxed cluster shapes are not found to be significantly affected by that correction. Therefore, dispersion forces have not been taken into account further.

2.2. Parametrisation and validation of the VMG force field

The 27 coefficients in Eq. 3 and the two parameters which tune the smoothness of the metallic coordination (Eq. 4) are fitted to reproduce the DFT adhesion energy, E_{adh}

(Eq. 5). At empirical level, the metal-metal interactions within the nanoparticle are modelled within a second moment approximation tight-binding potential, which has been extensively used for the study of free and supported nanoparticles [45, 46] and it is able to reproduce geometrical deformation/transition in metallic and bimetallic nanoparticles [12]. The adhesion energy is calculated for at least six different heights of the metallic cluster away from the substrate, and at different lateral (x, y) displacements: (1) no displacement (0,0) corresponding to most metal atoms on top of oxygen (O-site); (2) (a/2,a/2) corresponding to most metal atoms on top of magnesium (Mg-site); (3) (a/2,0) corresponding hollow surface site between oxygen and magnesium ions (hollow-site). As the energetically optimal position of the cluster in z-direction changes for different (x_i, y_i) positions, the following displacements along z are considered: $\pm$ 0.3 , $\pm$ 0.2 , $\pm$ 0.1 and 0 (O-site); 0.2 to 1.6 at 0.2 intervals (Mg-site); 0.2 to 1.0 at 0.2 intervals (hollow-site). This way, we make sure that the potential energy minimum is captured with sufficient number of points on both sides. Fitting of Eq. 1 is then performed by fixing the coordination cut-off Eq. 4 to the O-O distance of the substrate (r_c = 2.9755 Å), while search for optimal values of m together with the parameter r_c is carried out using basin-hopping Monte Carlo optimisation algorithm [40]. The robustness of the proposed parametrisation is checked versus the direct comparison of the adhesion energy for five architectures, where both (100) and (111) epitaxy are explicitly considered, as the $TO_{38}^{(100)}$, $TO_{38}^{(111)}$, $CO_{55}^{(100)}$, $CO_{55}^{(111)}$, $Ih_{55}^{(111)}$, $Dh_{58}^{(111)}$ as well as $Dh_{75}^{(111)}$, as reported in Fig. 2.2.

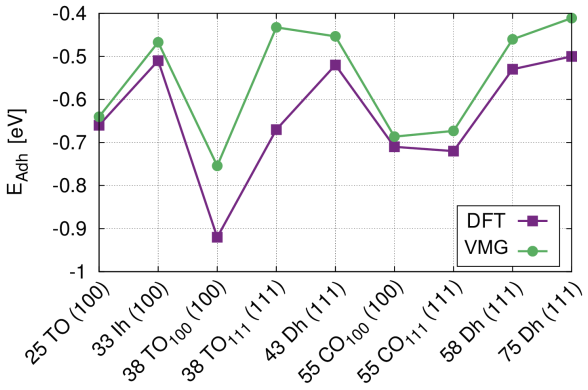

Figure 2. The adhesion energy E_{ads} per interfacial atom ($N_{interface}$) for various Pt nanoparticles depicted in Fig.2 as calculated by the two level of the theory. Per each structure, we provide the index to identify the type of the facet at the interface.

The agreement between the DFT and EP level calculated adhesion energies is very good, though there are some clear exceptions, as for the $TO_{38}^{(100)}$ and the $TO_{38}^{(111)}$. They seem to be due to (i) few interfacial atoms (only four for the former, which are symmetrically equivalent); (ii) a different deformation after relaxation at the DFT and empirical level. We observe a linear dependency in the calculated E_{ads} values as a function of the number of metallic atoms at the interface. The adhesion energy per

contact atom is ~ 0.6 eV. Upon relaxation, the overall gas-phase geometry of the cluster of Pt supported systems display a distribution of epitaxial configurations due to atomic rearrangements. These range from having regular atomic over-hangings (TO_{38}, CO_{55} and Dh_{55} clusters), to large contact (wetting) angles (particularly for those clusters with extended interfacial areas such as TO_{25}). Uneven over-hangings, small contact angles and several re-entrances are observed for those clusters displaying more irregular arrangements (Ih_{19} to Ih_{55}), as well as Dh_{43}, Dh_{58} and Dh_{75}). The calculated cluster average height to the substrate resembles that of monolayer (ML) cases: 2.279 Å for Pt on top of an O. Deviations from this reference value are observed for the larger cluster sizes as not all metal atoms lie on top of O-sites, and at some surface sites such as Mg, heights of nearly 2.62 Å can be expected. Our calculated bulk Pt lattice constant is 3.977 Å (cohesive energy E_{coh} value is 5.52 eV). This creates a small lattice mismatch for Pt of the order of 5%. Hence, the larger Pt-Pt bond length implies that for the vast majority of the (100) interfaces have relatively low roughness values compared to the more compact (111) ones.

3. Results

We probe the thermodynamic stability of Pt icosahedral clusters of 561 atoms (~ 3 nm) previously relaxed in the gas phase, and then soft-landed upon a MgO(100). We adopt an iterative increasing temperature MD scheme, where the temperature, controlled by an Andersen thermostat, is increased by 50 K every 10 ns, ensuring a melting rate as slow as 5 K/ns. After a temperature increment, the system is left free to move per each temperature accordingly to Newton's equations of motion, integrated using the velocity-Verlet algorithm with a time step of 5 fs. The overall temperature range explored is 350-1500 K, although a few extra simulations were carried out between 700-1500 K. We perform at least 7 Molecular Dynamics simulations to gather sensible statistics.

In Fig. 3 we report the caloric curve per each single run (gold lines) and their average (purple line) to capture the thermodynamical behaviour of the system, where we consider the excess energy $\Delta E = E_{coh} * N = E_{pot}/N^{2/3}$ with E_{coh} is the cohesive energy of the metal, E_{pot} the potential energy of the cluster and N the number of atoms in it. We observe two transitions characterized by negative specific heat (a sharp drop in the caloric curve) around 650 K and just below 950 K. The first one ties in with the transition of the interface layer towards a (100) arrangement and a square shape while the rest of the cluster maintaining an Ih architecture, the second one to the formation of a crystalline architecture, in agreement with the non continuous passage from non-crystalline to crystalline shape detected experimentally. [47] The melting transition of the cluster is instead characterised by a net departure from the linear temperature dependence of the caloric curve, which in all runs starts after 1500 K. The melting temperature, although still lower than the Pt-bulk limit (2041 K), is about 200 K higher than those of free icosahedral Pt-nanoparticles of identical size (1300 K).

To characterize quantitatively the pre-melting structural changes we employ two

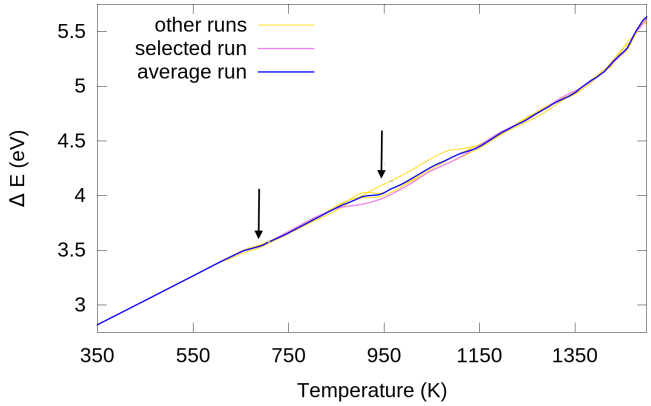

Figure 3. Caloric curves for an initial Pt_{561}^{Ih} cluster: each simulation is shown in yellow, while orange is used to plot the average behaviour and purple to distinguish the run analysed in Fig. 4.

geometrical descriptors. The common neighbour analysis (CNA) [48], which has been extensively used in the gas phase, enables to discriminate different atomic arrangements both in the inner and outer shells of the cluster. In particular, we look at the (555) signature which counts how many pairs of atoms belong to a five-fold axis. To have an insight on the evolution of the contour of the cluster, we slice the cluster in stripes of equal height (2.37 $\mathring{A}$) and enumerate the number of atoms in each layer. The former height was chosen as equal to the first peak of the pair distribution function multiplied by $\sqrt{(3)}/2$. This choice accounts for the five-fold axis 60° contact angle with respect to the pristine MgO(100) substrate.

To show in more detail how the two solid-solid transition take place, let us focus on a specific run, shown in Fig. 4. We remark that this is a paradigmatic example of the thermodynamical behaviour registered in all the simulations. Looking at the (555) signature, Fig 4 (a), we observe that the initial icosahedral structure is largely stable up to a temperature of 600-650 K. Initially the Pt_{561}^{Ih} cluster displays 11 layers, corresponding to the number of atoms on each five-fold axis. After landing, the base layer contains $\sim$ 20 atoms, the second layer $\sim$ 30, with a similar increase in atoms in subsequent layers until the sixth, that is the most populated, with $\sim$ 75 atoms. The number of atoms in the upper layers decreases in a similar way. To some extent, this implies that the cluster shape is a 'balloon' and the contact angles of all the facets are acute obtuse on average, as also shown by the first snapshots of Fig. 4 (b).

In the 650-700 K temperature range, the interface layer moves to match the O-sites in the substrate as evidenced by the decrease in the (555) signature percentage, but it is still almost triangular. Hence, we observe a significant increase of the population in the first three layers at the expanse of the top five ones, Fig 4 (c). The interface layer now has an almost square shape. In Fig. 4 (b), we report a snapshot of the cluster after the first structural transition, around $\sim$750 K: we highlight its hybrid morphology with a (100) square lowermost layer and an Ih cap. Until 950 K, the upper section

of the cluster shows an Ih morphology, however we observe a propagation of the (100) arrangement which leads to a decrease in the (555) signature percentage up from an original 2% to almost 0.5%. We highlight that a negative heat dilation is observed as long as the icosahedral cap is still present, in agreement with experimental results on similar systems. [15, 16]

For a temperature range of 800-950 K an almost continuous increment of the population in the lower four layers, together with the loss of the upper layers. A sharp increment of the 4th one and a slow constant growth of the lower ones and the contemporaneous disappearance of 5-fold symmetry axis in the clusters leads the full Ih→FCC transition, just before 950 K. After the full solid-solid structural transition, a structurally sounded cuboctahedral shape, presenting an alternation of (100) and (111) facets, is formed. Up to 1100 K, the new morphology appears stable, the few jumps in figure 4 bottom panel are either due to surface diffusion of atoms, or due to the partial reconstruction of the cluster towards a more favourable truncated octahedral architecture. These small reconstructions do not appear as significant features in the caloric curve.

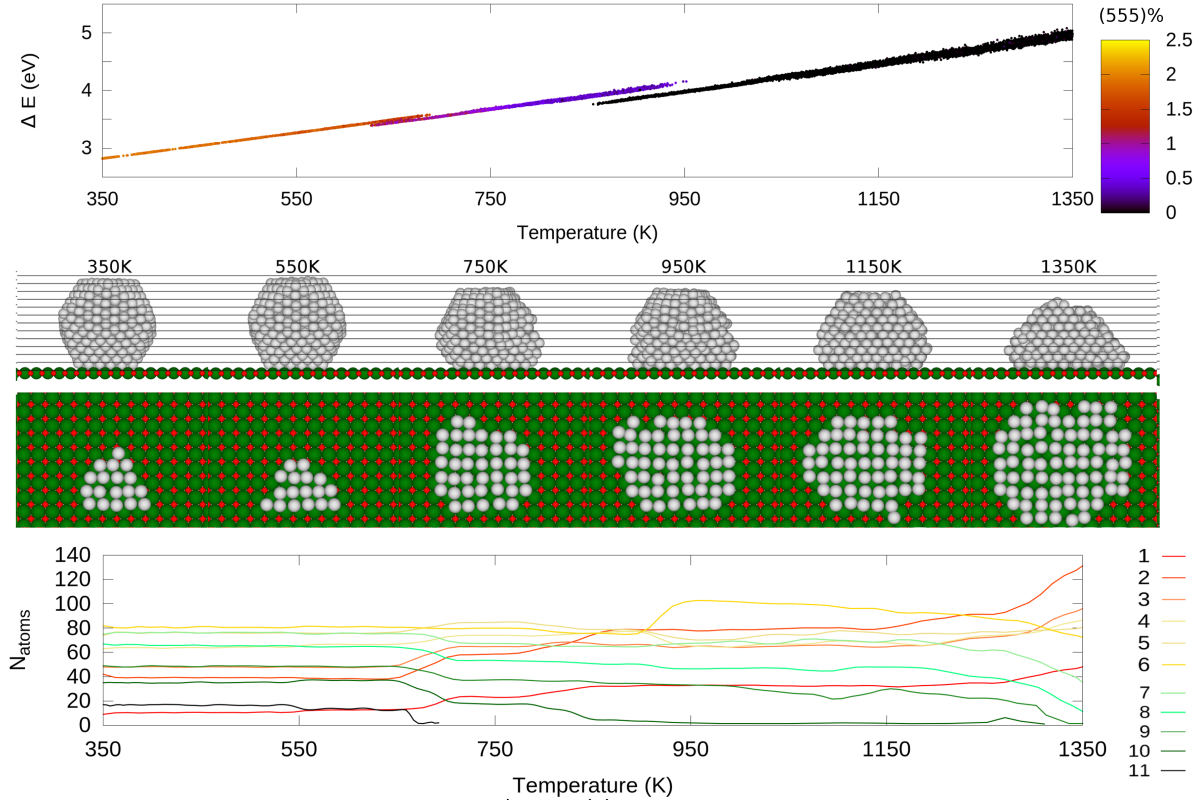

Figure 4. a) Caloric curve for the melting simulation reported in green in Fig. 3, (555) CNA signature percentage is reported in color. b) Snapshots taken during the aforementioned simulation, Pt atoms are in grey, Mg in green and O in red. Layers with an height of 2.37 *Å* are shown. c) Evolution of the number of atoms in each layer, with layer 1 being the lower one, with respect to temperature of the system.

Further we note another significant change in the nanocluster's morphology at 1150 K, when the first layers increase their population, up to 100 atoms for the first layer and above for the second and the third ones. Simultaneously, we observe the loss of two top layers as soon as the clusters to melt. The first layers populations suggests a change towards more acute contact angles and the formation of a 'haystack' shape. Interestingly, no drop in the caloric curve appears for this structural transition.

Finally, we would like to comment on the overall mobility of the Pt nanoparticles by analysing the motion of the centre of mass of the layer in contact with the oxide (COM_{base}). No changes of the COM_{base}'s coordinate are observed at low temperatures, a shift in its position of roughly one oxygen-oxygen distance is instead found at medium temperatures and a more dispersed but still not diffusive pattern at high temperatures is reported. The cause of the shift in COM_{base} position is due to atoms originally from higher layers dropping down. The centre of mass of the whole cluster moves in the same direction, which could be explained by the mismatch between the facet of the cluster at the interface and the substrate destabilising one side of the cluster more than the others. The lack of motion is observed in all the performed simulations, we thus predict that the diffusion of large Pt icosahedra is negligible on a oxide support: even during their rearrangements to have a (100) interface the center of mass shifts of one/two lattice spaces due to the enlargement of the interface facet.

4. Conclusion

We propose a new parametrisation for the VMG potential, as implemented in our classical Molecular Dynamics package.[49] The fitting of the force-filed parameters is in order to reproduce adhesion properties obtained at *ab-initio* level. Here we directly apply it for a 3 nm icosahedral Pt nanoparticle onto MgO(100). Our approach enables the study of thermal and geometrical features of Pt nanoparticles in a wide size range. It is capable of reproducing experimentally observed phenomena, such as the lack of diffusion of the cluster on the oxide substrate, and its wetting to the oxide as temperature increases. The heating up to the melting of the icosahedral platinum clusters shows also a fairly consistent reconstruction towards a bulk arrangement, which occurs at around ∼950 K, with a melting phase transition beginning above 1500 K, roughly 200 K above the free gas melting temperature. The reconstruction of the Ih towards a FCC polyhedra agrees with energetic arguments, being the latter more favourable on an MgO(100) substrate, at least in this size range. The morphological re-arrangement is not sharp and instantaneous and comprises intermediate and long-lived hybrid architectures, with a (100) interface and still a icosahedral upper half is observed between 700-950 K. We highlight that the intermediate architectures. observed before the structural transition in a TO, labelled as "squared interface + Ih", can be detected experimentally: it results to be stable in a wide range of temperatures and over several tens of ns. We expect such long-lived metastable minima to be present also during other Ih into FCC transition of oxide supported metallic nanoparticles. The formation of this kind of

hybrid morphology should be takein in account for their technological applications, as it may present peculiar properties between the one of icosahedral and FCC geometries.

4.1. Appendices

List of the new fitted parameters for Pt deposited on MgO(100).

4.2. Acknowledgments

FB, LP, LOPB thanks the financial support by U.K. research council EPSRC, under Grants No. EP/GO03146/1 and No. EP/J010812/1 while the studentship of KR is sponsored by EPSRC grant number ER/M506357/1. L.O.P.B. acknowledges PAPIIT-UNAM (Project IA 102716). IA and FB thanks the financial support offered by the Cost-Action MP0903 "Nanoalloy". All the authors thanks the financial support offered by Royal Society under the project number RG120207.

5. References

[1] G.G. Asara, L. O. Paz-Borbon, and F. Baletto. *ACS Catalysis*, 2016.
[2] C. DiPaola, R. D'Agosta, and F. Baletto. *NanoLett.*, 16:2885, 2016.
[3] F. Baletto and R. Ferrando. *Phys. Chem. Chem. Phys*, 17 (42):28256–28261, 2015.
[4] F.Calle-Vallejo, J. I. Martnez, J.M Garcia-Lastra, P. Sautet, and D. Loffreda. *Angewandte Chemie - International Ed.*, 53:8316, 2014.
[5] B. Roldan Cuenya and F. Behafarid. *Surface Science Reports*, 70:135, 2015.
[6] D.J. Wales and J.P.K. Doye. *JPC A*, 101 (28):5111–5116, 1997.
[7] R.L. Johnston. *Dalton Trans.*, 22:4193–4207, 2003.
[8] G. Rossi and R. Ferrando. *Journ. of Phys: Cond. Mat.*, 21(8):084208, 2009.
[9] A. S. Barnard. *Reports on Progress in Physics*, 73(8):086502, 2010.
[10] F. Baletto and R. Ferrando. *Rev. Mod. Phys.*, 77:371–423, 2005.
[11] Y. Yang and H. Zhang. *ACS Nano*, 8 (7):74657477, 2014.
[12] L. Pavan, K. Rossi, and F. Baletto. *J. Chem. Phys.*, 143:184304, 2015.
[13] A.C. Ngandjong, C. Mottet, and J. Puibasset. *J. Phys. Chem. C*, 120:8323, 2016.

Table 2. Values of the VMG coefficient $c_{\alpha,\beta,\gamma}$ as they appear in Eq. 3, obtained by the fitting and used in the above study. α, β, γ runs between 1 to 3.

0.289166	0.149843	0.045534
1.545652	0.046514	0.089767
2.742241	-0.261726	-0.004003
1.120724	0.278722	-0.015515
-0.027956	0.171355	-0.037242
-0.542610	0.109480	0.046956
1.168890	-0.103545	0.033496
2.282238	0.655619	0.280348
2.093507	-0.230162	0.193065

[14] C.S Ewing, G. Veser, J.J McCarthy, J.K. Johnson, and D.S. Lambrecht. *J. Phys. Chem. C*, 119:19934, 2015.
[15] F. D Vila, S. T. Hayashi, J. M. Moore, and J. J. Rehr. *J. Phys. Chem. C*, 120:14883, 2016.
[16] S. I. Sanchez, L. D. Menard, A. Bram, J. H. Kang, M. W. Small, R. G. Nuzzo, and A. I. Frenkel. *JACS*, 131:7040, 2009.
[17] C. Gan, W. Chuanjie, and Z. Peng. *Physics and Chemistry of Liquids*, 53:518, 2015.
[18] C. Mottet, J. Goniakowski, F. Baletto, R. Ferrando, and G. Treglia. *Phase Transitions*, 77:113, 2004.
[19] F. Ding, A. Rosn, S. Curtarolo, and K. Bolton. *Appl. Phys. Lett.*, 88:133110, 2006.
[20] S. C. Hendy. *Nanotechnology*, 18:175703, 2007.
[21] D. Schebarchov, S.C. Hendy, and W. Polak. *J. Phys. Condens. Matter*, 21(14):144204, 2009.
[22] Y. Lan, S. Chiu-Hun, S. Wen-Hsien, and S. An-Chung. *RSC Adv.*, 4:13768, 2014.
[23] A. Tal, E. Peter Münger, and I. A. Abrikosov. *Phys. Rev. B*, B92:020102(R), 2015.
[24] K. Rossi, L. Pavan, Y.Y Soon, and F. Baletto. *submitted*, 2016.
[25] M. Ahmadi, F. Behafarid, and B. Roldan Cuenya. *Nanoscale*, 8:11635, 2016.
[26] B. Roldan Cuenya. *Acc. Chem. Res.*, 46(8):1682–91, 2013.
[27] A. Jelea, C. Mottet, J. Goniakowski, G. Rossi, and R. Ferrando. *Phys Rev B*, 79:165438, 2009.
[28] A. I. Frenkel, M.W. Small, J.G. Smith, R.G Nuzzo, K.O. Kvashnina, and M. Tromp. *J. Phys. Chem. C*, 117:23286–23294, 2013.
[29] Y.Han, R. Ferrando, and Z. Li. *J. Phys. Chem. Lett.*, 5(1):131–137, jan 2014.
[30] E. Carrasco, M. A. Brown, M. Sterrer, H. J. Freund, K. Kwapien, M. Sierka, and J. Sauer. *J. Phys. Chem. C*, 114:18207, 2010.
[31] H. Wang, R. G. Tobin, D. K. Lambert, C. L. DiMaggio, and G. B. Fischer. *Surf. Scie.*, 372:267, 1997.
[32] R. Ferrando, G. Rossi, A.C Levi, Z. Kuntova, F. Nita, A. Jelea, C. Mottet, G. Barcaro, A. Fortunelli, and J. Goniakowski. *Journal Chem. Phys.*, 130:174702, 2009.
[33] W. Vervisch, J. C. Mottet, and Goniakowski. *Phys. Rev. B*, 65(24):245411, 2002.
[34] J .Goniakowski and C. Mottet. *Phys. Rev. B*, 2010.
[35] S.M Kozlov, H.A. Aleksandrov, J. Goniakowski, and K.M. Neyman. *J. Chem. Phys.*, 139(8), 2013.
[36] S. Sao-Joao, S. Giorgio, C. Mottet, J. Goniakowski, and C.R. Henry. *Surf. Sci.*, 600(7), 2006.
[37] R. Ferrando, G. Barcaro, and A. Fortunelli. *Phys. Rev. Lett.*, 102(May):216102, 2009.
[38] J. Goniakowski, A. Jelea, C. Mottet, G. Barcaro, A. Fortunelli, Z. Kuntová, F. Nita, A.C. Levi, G. Rossi, R. Ferrando, and J. Goniakowski. *J. Chem. Phys.*, 130:174703, 2009.
[39] J. Olander, R. Lazzari, J. Jupille, B. Mangili, and J. Goniakowski. *Phys Rev B*, 76:075409, 2007.
[40] I. Atanasov, G. Barcaro, F.R. Negreiros, A. Fortunelli, and R.L. Johnston. *J. Chem. Phys.*, 138:224703, 2013.
[41] P. Giannozzi, S. Baroni, N. Bonini, M. Calandra, R. Car, C. Cavazzoni, D. Ceresoli, G.L. Chiarotti, M. Cococcioni, I. Dabo, A. Dal Corso, S. de Gironcoli, S.Fabris, G. Fratesi, R. Gebauer, U. Gerstmann, C. Gougoussis, A. Kokalj, M. Lazzeri, L. Martin-Samos, N. Marzari, F. Mauri, R.Mazzarello, S. Paolini, A. Pasquarello, L. Paulatto, C. Sbraccia, S. Scandolo, G. Sclauzero, A. P. Seitsonen, A. Smogunov, P Umari, and R. M. Wentzcovitch. *J. Phys. Condens. Matter*, 39:395502, 2009.
[42] J.P. Perdew, K. Burke, and M. Ernzerhof. *Phys. Rev. Lett.*, 77(18):3865, 1996.
[43] S. Grimme. *J. Comput. Chem.*, 27:1787, 2006.
[44] G. Ramos-Sanchez and P.B. Balbuena. *Phys. Chem. Chem. Phys*, 15:11950, 2013.
[45] F. Baletto, R. Ferrando, A. Fortunelli, F. Montalenti, and C. Mottet. *The Journal of Chemical Physics*, 116(9):3856, mar 2002.
[46] and C. Mottet, J. Goniakowski, F. Baletto, R. Ferrando, and G. Treglia. *Phase Transitions*, 77:101, 2004.
[47] L. Li, L. Wang, D. Johnson, Z. Zhang, S. I. Sanchez, J. H. Kang, R. G. Nuzzo, Q. Wang, A. I. Frankel, J. Li, J. Ciston, E. A. Stach, and J. C. Yang. *J. Am. Chem. Soc.*, 135:13062, 2013.

[48] J. D. Honeycutt and H.C. Andersen. *J. Chem. Phys.*, 1987.
[49] F.Baletto et al. *in preparation.*